Segregation and Clustering of Ash in Volcanic Plumes and Clouds

Genesis of Accretionary Lapilli

Roger P. Denlinger[1], Alexa van Eaton[1] and Þórður Arason[2]
roger@usgs.gov, avaneaton@usgs.gov, arason@vedur.is

Abstract

Volcanic plumes are energetic, turbulent flows of particles and gas that produce aggregates, accretionary lapilli, when the plumes contain liquid water. Lapilli often have a chaotic, coarser-grained core surrounded by finer-grained outer rims. Accretionary lapilli are found in diverse eruption deposits around the world, yet they show similar internal structures. Using decades of research in gas-particle flows, we show that these structures reflect the turbulent structure of each plume that produced them. Particle clustering and size segregation are ubiquitous in highly turbulent gas flows carrying solid particles such as volcanic plumes. Injected into laboratory gas jets, particles become segregated and form clusters of similar sizes by interacting and modulating the turbulent structure of the flow that carries them. Carried in suspension, the *size* of solid particles or aggregates is much more important than either their shape or density. We use this knowledge to analyze the formation of accretionary lapilli and ashy hailstones from two eruptions in which there is evidence of liquid water in the plume—the March 23, 2009 eruption of Redoubt Volcano, Alaska, and the 2011 eruption of Grímsvötn volcano, Iceland. At Grímsvötn, large clear hailstones contained clumps of fine ash, and individual particles distributed eccentrically within the stones indicate that the stones picked up the ash at random during transport. At Mt. Redoubt, with textural features of lapilli and other tephra, weather radar observations, and ATHAM numerical simulations of the plume, we were able to determine the eddy structure in the plume that carried and formed the lapilli sampled in the deposits produced by this eruption.

Scaling of turbulent flows, with or without particles

We determine the rate of dissipation of turbulent kinetic energy by assuming that the rate of production of turbulent kinetic energy by the largest eddies is balanced by the rate at which it is destroyed or dissipated by viscosity in the flow. Turbulent energy is transferred from large eddies to small eddies, forming an energy cascade. The rate of dissipation controls the spatial frequency spectrum of this energy cascade, as shown in **Figure 1** [*Pope*, 2000]. Whereas the turbulence in the largest structures is anisotropic, in high Reynolds number flows breakup of large eddies results, at some finer scale (typically on the order of 1/10 of the width of a plume), in a universal isotropic and largely homogeneous turbulence structure that is defined by the rate of kinetic energy transfer and dissipation [*Pope*, 2000]. The foundation of this dissipation scaling is the *Richardson-Kolmogorov cascade*, which states that the rate of energy dissipation is proportional to the product of turbulent kinetic energy and average fluctuation velocity divide by some turbulent length scale (*lo* in **Figure 1a**).

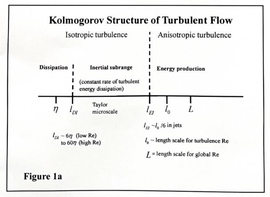

Figure 1a

Laboratory jets (small scale, low Re) versus Volcanic plumes (large scale, high Re)

Laboratory flows, with lower Reynolds numbers, have much narrower ranges of eddy sizes to couple with particles than do large-scale volcanic plumes [*Denlinger et al., submitted*] or atmospheric flows [*Siebert et al., 2006*] . We can test theories of gas-particle coupling with laboratory experiments backed up by numerical simulations of the same experiments; here we compare DNS results (**Figure 3**) with ATHAM results (**Figure 8**). The scaling of this comparison is shown in **Figure 1b** and **1c**.

Experimental and Numerical Tests of jets with particles

In numerical and experimental simulations of self-similar jets with particles the turbulence of the gas-solid suspension varies within the jet. Using DNS, *Li et al.* [2011] investigates both particle-free and particle laden jets, with Re~1700, and their results (**Figure 3**) correspond closely to the experimental results of *Yuu et al.* [1996]. In both numerical and experimental round jets, the turbulence becomes modulated as particles are added. In the particle-laden jet here, the volume fraction is about 10^{-5} and eddies are altered by particles in 2-way coupling to produce both segregation and clustering of particles in the flow. This coupling varies with particle size. Only the finest sizes in the simulations produced clustering and segregation (**Figure 3a**). The variations between panels are predicted by the limits based on ***St()*** which states that *full coupling only occurs for* **$0.6 < St() < 6$**.

Significance for aggregation:

These studies show that the separate paths taken by particles with different response times and ***St()*** numbers provide a mechanism for rapid and efficient collisions between particles of different sizes (travelling on intersecting paths), impacting aggregation. To assess aggregation in a gas-particle flow with a range of particle sizes, we studied clear hailstones produced by Grímsvotn that had collected ash particles as well as clumps of ash as they grew.

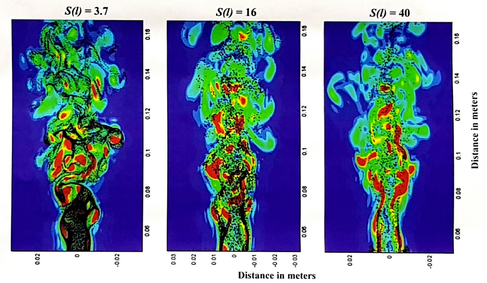

Figure 3. *Results of DNS study of Li, et al. [2011] which accurately simulated experimental results of Yuu et al. [1996]. Particle size increases from right to left, all other flow parameters are equal, and volume fraction is about 10^{-5}. Variations in the degree to which particles are coupled to the flow are evident, and agree with the St() number limits. Permission to use figure obtained from International Journal of Multiphase Flow.*

Analysis of accretionary lapilli from Redoubt volcano produced during the March 23, 2009 eruption

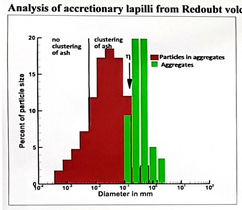

Figure 5. Grain size distributions for ash particles in aggregates and for aggregate and lapilli rims recovered from all tephra deposits sampled at various distances for the March 23, 2009 eruption of Redoubt volcano, Alaska.

Table 1. Analysis of frozen lapilli sampled approximately 12 km from the vent (see **Figure 5**). Nearly 20% of all aggregates formed during this short eruption had at least one internal rim, and 8% also had a core of larger crystals.

Description	Percentage	Image
Poorly sorted interior No inner rims	82.5%	
Poorly to moderately sorted interior Single inner rim	9.6%	
Cluster of large to medium size particles in core Single to multiple inner rims	7.9%	

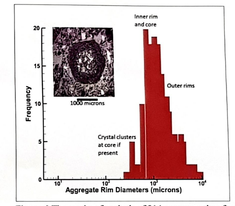

Figure 6. The results of analysis of 214 aggregate rims from Table 1, some which are internal as shown in the inset. Outer rims were typically formed of much finer ash. In those cases like the inset above, clustered large crystals form a core.

Radar Data

Figure 7a. Backscatter C-band radar images of the March 23, 2009 eruption of Redoubt volcano in Alaska that began at **12:30:21**. From left to right, images are about five minutes apart. The grid lines are at 5 km both vertically and horizontally, showing a 1.6:1 vertical exaggeration. These are compared with snapshots of ATHAM model runs at the same times and scales.

DNS Gas-Particle Jet Simulation of Li et al., (2011)

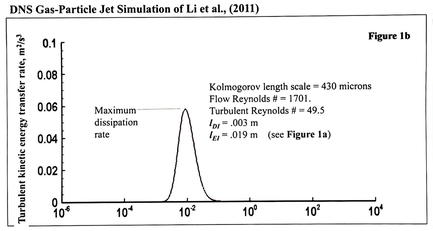

ATHAM simulation of March 23, 2009 eruption of Mt. Redoubt, Alaska

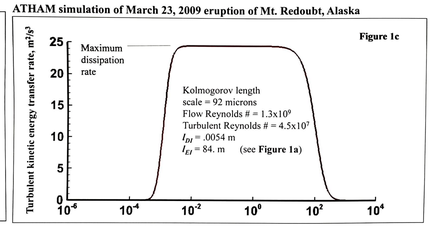

Mechanics of turbulent gas suspensions of solid particles

The primary factor that determines the nature of particle modulation of turbulent gas-solid suspensions is the solid volume fraction, or the volume of solid, dense particles per unit volume of gas [*Said Elghobashi*, 2004a; *Saber et al.*, 2015]. For turbulent gas-solid suspensions, three broad categories of coupling are defined (**Figure 2**); one-way coupling, two-way coupling, and four-way coupling [*Said Elghobashi*, 2004a; *Saber et al.*, 2015].

One-way coupling occurs for volume fractions less than 1 ppm, and is passive transport. Particles of any size carried by the gas (or falling through it) do not modify its turbulent structure in any significant way. This is the mechanism of transport in distal ash clouds.

Two-way coupling occurs when volume fractions are between 1 ppm and one part per thousand. In two-way coupling, the suspension is volumetrically dilute, but the particles interact with the carrier fluid and change the turbulent structure of the flow. With a mixture of particle sizes, the particles become segregated and clustered by size in the flow. larger clusters and particles sweep through small eddy structures, acquiring the smaller particles and clusters trapped between them. This is active in all plumes and some proximal ash clouds.

Four way coupling occurs for large volume fractions in excess of one part per thousand, where bulk momentum transport, in addition to turbulence modulation, is significantly affected by frequent particle collisions. Radar measurements of volcanic plumes [*Marzano, et. al, 2013; Schneider and Hoblitt, 2013*] show that this volume concentration, for any particle size, is ephemeral at best in volcanic plumes, and is often only recorded for short times (< 1 minute) and near the vent.

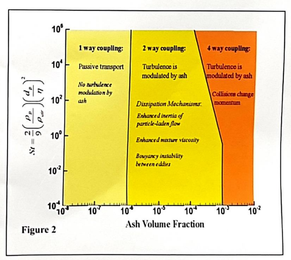

Figure 2

Scaling gas-particle coupling:

Each particle or aggregate size suspended in turbulent gas is coupled to a range of eddy sizes, depending upon the ratio of particle response time relative to the turnover time of eddies in the flow, defined here as ***St()***. This scaling explains variations in clustering of different size particles observed in experiments and obtained in DNS simulations (**Figure 3**), variations that cannot be explained with the common Stokes equation shown in **Figure 2** [*Goto and Vassilicos*, 2006; *Monchaux et al.*, 2012; *Vassilicos*, 2015]. This ***St()*** ratio, and the range of eddy sizes that result from it, are given by the following expressions:

$$l_{\min} = 7.123 \cdot 10^{-3} \left(\frac{\rho_{solid}}{\rho_{gas}}\right)^{\frac{3}{2}} \left(\frac{d_p^3}{\eta^2}\right) \qquad l_{\max} = 0.225 \cdot \left(\frac{\rho_{solid}}{\rho_{gas}}\right)^{\frac{3}{2}} \left(\frac{d_p^3}{\eta^2}\right) \qquad S(l) = \frac{2}{9}\left[\frac{\rho_{particle}}{\rho_{gas}}\right]\left[\frac{d_p^2}{l^{2/3}\eta^{4/3}}\right]$$

l = eddy size (m)
d_p = particle or aggregate diameter (m)
ρ = solid or gas density (kg/m³)
η = Kolmogorov scale (m)

Ash-infused hail from Grimsvotn in 2011

At Grimsvotn in 2011, hailstones swept through a volcanic plume and cloud, collecting ash, and were transported and deposited about 3 km from the vent. Þórður Arason sampled and photographed this deposit shortly after it was produced (Figure 4). Radar measurements of the plume producing this hail [*Petersen et al.*, 2012] show that particle volume concentrations were less than 10^{-3}, so 2-way coupling dominated particle interactions in this gas-solid suspension. The hailstones in the photograph were measured with ImageJ, and the ash visible in each hailstone was examined. Most hailstones had ash inclusions of various sizes, some clearly formed from clusters of smaller ash particles, and the inclusions are distributed eccentrically in the round hailstones. The sizes seen in the ash inclusions in the photo are larger than single grains visible in the image, supporting the view that the hailstones swept through the plume or cloud, incorporating ash and clusters of ash as they grew. This is the same mechanism proposed by *Van Eaton et al.* [2015] for the March 23, 2009 eruption (event 5) at Mt. Redoubt, Alaska.

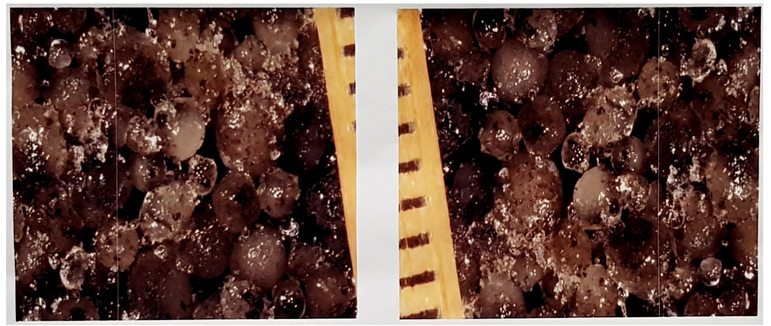

Figure 4. *Hailstones photographed by Þórður Arason with a flash and a macro lens on 11 June 2011 at 12:20 UTC in situ in a ditch through the ash layer at 64°22.497'N, 17°25.019'W, 1570 m a.s.l., 3.0 km SSW of the vent. The scale on the margins shows ticks at 1 mm intervals. Temperature measurements at Grimsfjall (6 km to the E) indicate that air temperatures were below freezing from the start of the eruption to this time. Irregular fragments of ash are small and isolated within a small portion of the near surface of each round hailstone. These fragments are larger than the ash particles forming them, and in most cases are clusters of ash rather than particles. Individual clusters can also be seen within clouds of ash near the surface of some larger stones.*

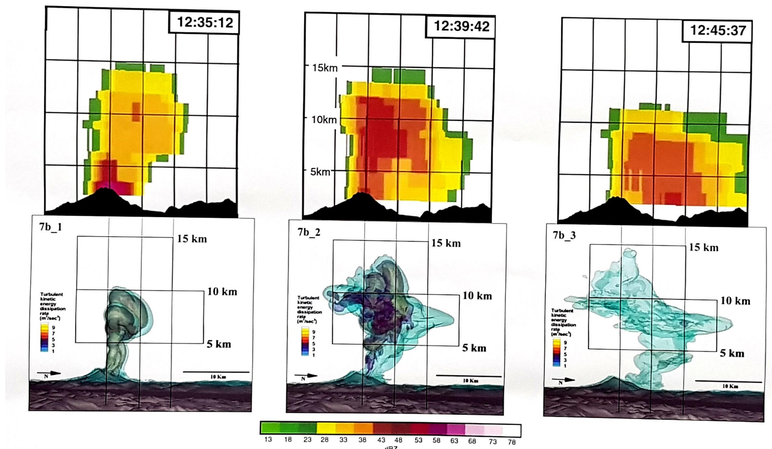

Fig 7b. ATHAM images of the growth (**7b_1**), full bloom (**7b_2**), and decay (**7b_3**) of internal eddy structures in the eruption plume for the March 23, 2009 eruption. The innermost two surfaces enclose the homogeneous turbulence of the inertial subrange (**Figure 1a**), and are compared to backscatter images from radar data in **Figure 7a** at the same times and the same scale. The inertial subrange is where most of the lapilli in **Figure 6** first cluster and begin to grow, and is where the transfer rate of turbulent kinetic energy from large to small eddies is at a maximum. There are three nested model surfaces shown in each figure, corresponding to three kinetic energy dissipation rates (0.1, 5, 10), and all surfaces are largely internal to the actual and radar-measured plumes. The areas of high backscattered energy in the radar images are dark orange and red, and correspond to locations in these images where **ATHAM** solutions project locations of maximum rates of turbulent kinetic energy dissipation (at least 5 m^2/sec^3). Many areas in the radar below 6 km correspond to ash in deposition. After the eruption stopped at about **12:36:00**, the eddy structure began to decay back to that of the atmospheric wind field, gradually losing the capacity to suspend ash and increasing ash deposition.

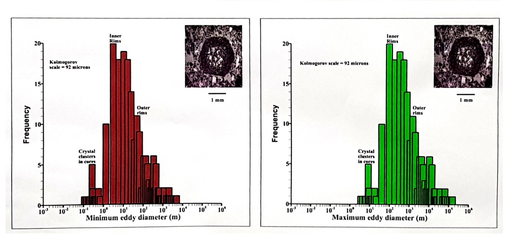

Figure 8. The rim sizes of the accretionary lapilli, combined with the energy scaling from **ATHAM** simulations for the March 23, 2009 event [*Van Eaton et al.*, 2015], produces this eddy size distribution within the dark orange to red areas in the three panels in **Figure 7a** and the red and purple regions in the corresponding panels in **Figure 7b**. The two plots to the right, from the data in **Figure 6**, show that the cores and inner rims begin to form in the inertial subrange shown in **Figure 1c**, but as lapilli grow they are increasingly carried by large, anisotropic eddies in the flow that are maintained by continued eruption [*Denlinger et al., to be submitted*].

Denlinger, R.P., A. van Eaton, and P. Arason, Segregation and clustering of volcanic ash in volcanic plumes and clouds, to be submitted to Earth Planetary Science Letters.
Elghobashi, S. (2004a), An Updated Classification Map of Particle-Laden Turbulent Flows, paper presented at IUTAM Symposium on Computational Approaches to Multiphase Flow, Springer, Argonne National Laboratory.
Elghobashi, S. (2004b), An Updated Classification Map of Particle-Laden Turbulent Flows, paper presented at IUTAM Symposium on Computational Approaches to Multiphase Flow, Springer, Argonne National Laboratory. doi:10.1063/1.2364203.
Goto, S., and J. C. Vassilicos (2006), Self-similar clustering of inertial particles and zero-acceleration points in fully developed two-dimensional turbulence, Physics of Fluids, 18(11), 115103, doi:10.1063/1.2364203.
Kolmogorov, A. N. (1962), A refinement of previous hypotheses concerning the local structure of turbulence in a viscous incompressible fluid at high Reynolds number, Journal of Fluid Mechanics, 13, 82-85.
Li, D., J. Fan, K. Luo, and K. Cen (2011), Direct numerical simulation of a particle-laden low Reynolds number turbulent round jet, International Journal of Multiphase Flow, 37(6), 539-554, doi:10.1016/j.ijmultiphaseflow.2011.03.013.
Mando, M., M. F. Lightstone, L. Rosendahl, C. Yin, and H. Sorensen (2009), Turbulence modulation in dilute particle-laden flow, International Journal of Heat and Fluid Flow, 30, 331-338.
Marzano, F. S., E. Picciotti, M. Montopoli, and G. Vulpiani (2013), Inside Volcanic Clouds: Remote Sensing of Ash Plumes Using Microwave Weather Radars, Bulletin of the American Meteorological Society, 94(10), 1567-1586, doi:10.1175/bams-d-11-00160.1.
Monchaux, R., M. Bourgoin, and A. Cartellier (2012), Analyzing preferential concentration and clustering of inertial particles in turbulence, International Journal of Multiphase Flow, 40, 1-18, doi:10.1016/j.ijmultiphaseflow.2011.12.001.
Petersen, G. N., H. Bjornsson, P. Arason, and S. von Löwis (2012), Two weather radar time series of the altitude of the volcanic plume during the May 2011 eruption of Grímsvötn, Iceland, Earth System Science Data, 4(1), 121-127, doi:10.5194/essd-4-121-2012.
Pope, S. B. (2000), Turbulent Flows, 771 pp., Cambridge University Press, Cambridge, UK.
Saber, A., T. S. Lundström, and J. G. I. Hellström (2015), Turbulent Modulation in Particulate Flow: A Review of Critical Variables, Engineering, 07(10), 597-609, doi:10.4236/eng.2015.710054.
Schneider, D. J., and R. P. Hoblitt (2013), Doppler weather radar observations of the 2009 eruption of Redoubt Volcano, Alaska, Journal of Volcanology and Geothermal Research, 259, 133-144, doi:10.1016/j.jvolgeores.2012.11.004.
Siebert, H., K. Lehmann, and M. Wendisch (2006), Observations of small-scale turbulence and energy dissipation rates in the cloudy boundary layer, Journal of Atmospheric Sciences, 63, 1451-1466.
Vallis, G. K. (2006), Atmospheric and oceanic fluid dynamics, Cambridge University Press.
Van Eaton, A. R., L. G. Mastin, M. Herzog, H. F. Schwaiger, D. J. Schneider, K. L. Wallace, and A. B. Clarke (2015), Hail formation triggers rapid ash aggregation in volcanic plumes, Nat Commun, 6, 7860, doi:10.1038/ncomms8860.
Vassilicos, J. C. (2015), Dissipation in Turbulent Flows, Annual Reviews of Fluid Mechanics, 47, 95-114.
Yuu, S., K. Ikeda, and T. Umekage (1996), Flow-field prediction and experimental verification of low Reynolds number gas-particle turbulent jets, Physicochemical Engineering Aspects, 109, 13-27.

[1] **US Geological Survey**
1300 SE Cardinal Ct., Vancouver, WA 98683, USA
www.usgs.gov

[2] **Veðurstofa Íslands – Icelandic Meteorological Office**
Bústaðavegur 9, IS-108 Reykjavík, Iceland
www.vedur.is

IAVCEI 2017 Scientific Assembly, 14-18 August 2017, Portland, Oregon, USA
Poster VO43A-145